


ISSN: 0095-8972 (Print) 1029-0389 (Online) Journal homepage: <http://www.tandfonline.com/loi/gcoo20>


Structural and catalytic performance of a polyoxometalate-based hybrid compound

Lian-He Wu, Liang Li, Yan Zhao, Jing-Quan Sha, Dong-Wen Wang, Xiao-Ning Yang & Xiao-Qiu Wang

To cite this article: Lian-He Wu, Liang Li, Yan Zhao, Jing-Quan Sha, Dong-Wen Wang, Xiao-Ning Yang & Xiao-Qiu Wang (2015) Structural and catalytic performance of a polyoxometalate-based hybrid compound, *Journal of Coordination Chemistry*, 68:5, 766-776, DOI: [10.1080/00958972.2015.1009907](https://doi.org/10.1080/00958972.2015.1009907)


To link to this article: <http://dx.doi.org/10.1080/00958972.2015.1009907>

 View supplementary material [↗](#)

 Accepted author version posted online: 22 Jan 2015.
Published online: 13 Feb 2015.

 Submit your article to this journal [↗](#)

 Article views: 53

 View related articles [↗](#)

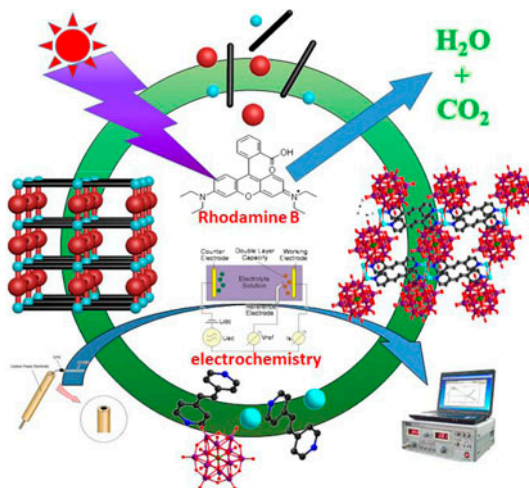
 View Crossmark data [↗](#)

Structural and catalytic performance of a polyoxometalate-based hybrid compound

LIAN-HE WU, LIANG LI, YAN ZHAO, JING-QUAN SHA*, DONG-WEN WANG,
XIAO-NING YANG and XIAO-QIU WANG

The Provincial Key Laboratory of Biological Medicine Formulation, Jiamusi University, Jiamusi,
PR China

(Received 17 September 2014; accepted 8 January 2015)



A new POM-based compound with *CDS* topology is reported, which displays good electrocatalytic and photocatalytic activities.

By introducing long rigid ligands into polyoxometalate (POM) systems, a new POM-based hybrid compound with *CDS* topology, $\{[\text{Cu}(\text{bpe})]_2(\text{H}_2\text{SiMo}_{12}\text{O}_{40})\} \cdot (\text{bpe}) \cdot 2\text{H}_2\text{O}$ (**1**) (bpe = bis(4-pyridyl) ethylene), has been hydrothermally synthesized and characterized by physical methods. Single-crystal X-ray diffraction analysis shows that the ladder-like 1-D structure of **1** is formed from Keggin clusters modified by the wavy $[\text{Cu}(\text{bpe})]_n$ chains. Compound **1** contains two types of tunnels along the *a* axis and the $[1-10]$ axis, which are occupied by isolated bpe molecules. Compound **1** bulk-modified carbon paste electrode (**1**-CPE) displays good electrocatalytic activity toward the reduction of nitrite and bromate, and photocatalytic activities indicate that **1** presents good degradation activity and may be a photocatalyst to decompose some organic dyes.

Keywords: Polyoxometalates; bpe; Electrocatalytic activity; Photocatalytic activity

*Corresponding author. Email: shajq2002@126.com

1. Introduction

The synthesis and characterization of coordination polymers (CPs) based on self-assembly of specifically designed building blocks has received attention [1–4]. The motivation behind much of this activity has been provided by the prospect of generating a wide range of designed materials with desired structures and useful properties such as electronic, magnetic, optical, and catalytic. Polyoxometalates (POMs), as one kind of well-defined metal oxide clusters with nanosizes, abundant topologies, and potential applications in catalysis, magnetism, and materials science [5–8], are widely used as inorganic building blocks to construct hybrid compounds [9–13]. Hybrids made of POMs associated with various CPs (named as POMCPs) have been reported, in which the CPs provide charge compensation and/or become a part of the inorganic POM framework. A survey of the literature reveals that POMs have been incorporated into CPs as pillars [14], templates [15] and participate in the formation of POMCPs [16]. However, in most cases, the architectures of POMCPs possess close accumulation model because of the interpenetrating, the interlocking, or the larger size of POMs, which hinders their study and applications in materials science.

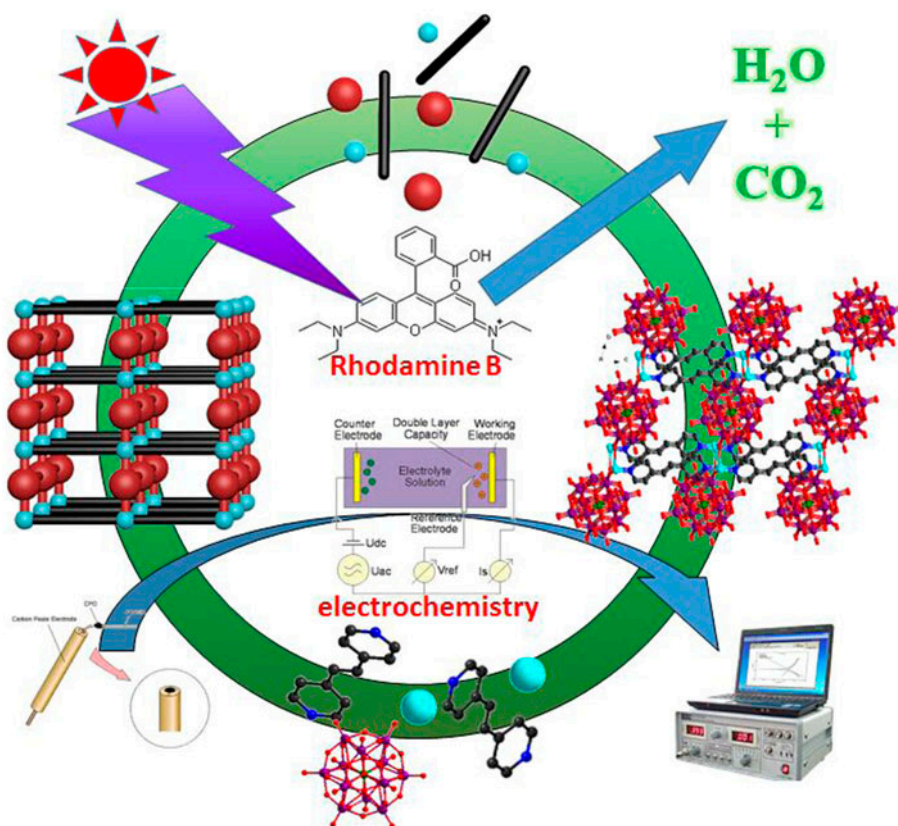
Research has focused on the application of POMCPs in 3-D bulk-modified carbon paste electrodes (CPE) by direct mixing [17–19], which has been widely applied in electrochemistry with advantages: inexpensive, easy to handle, and easy to prepare [20, 21]. Studies have also shown that POMCPs possess some active physical properties, in particular excellent photochemical nature makes them green photocatalysts for the reduction of environmental pollution [22, 23]. Many organic pollutant compounds can be degraded and removed by light-excited POMs with high oxidizing ability [24–26]. However, inherent drawbacks, such as high solubility in aqueous solution or low stability under catalytic conditions, limit the scope of practical applications [27–29]. So, a current development in the area is to explore stabilized lattice architectures resulting from the association of CPs and POMs.

To seek efficient and stabilized catalysts, herein, we selected Keggin POMs, bpe, and Cu ions to synthesize a new POMCP, $\{[\text{Cu}(\text{bpe})]_2(\text{H}_2\text{SiMo}_{12}\text{O}_{40})\} \cdot (\text{bpe}) \cdot 2\text{H}_2\text{O}$ (**1**). The new POMCP exhibits good electrocatalytic and photocatalytic activities (scheme 1). Bpe was selected to act as longer spacer ligands with good N-donor and to avoid interpenetrating and interlocking.

2. Experimental

2.1. Materials and general methods

All reagents were purchased commercially and used without purification. Elemental analyses were performed on a Perkin-Elmer 2400 CHN Elemental Analyzer (C, H, and N) and on a Leaman inductively coupled plasma spectrometer (Cu). IR spectra were obtained on an Alpha Centaur FT/IR spectrometer with KBr pellet from 400 to 4000 cm^{-1} . The TG analyses were performed on a Perkin-Elmer TGA7 instrument in flowing N_2 with a heating rate of 10 $^\circ\text{C min}^{-1}$. UV–vis absorption spectra were recorded on a 756 CRT UV–vis spectrophotometer. Cyclic voltammograms were obtained with a CHI 660 electrochemical workstation at room temperature. Platinum gauze was used as a counter electrode and Ag/AgCl electrode was the reference. Chemically bulk-modified CPE were used as working electrodes.



Scheme 1. Schematic representation of POMCPs with good electrocatalytic and photocatalytic activities.

2.2. Synthesis of $\{[Cu(bpe)]_2(H_2SiMo_{12}O_{40})\} \cdot (bpe) \cdot 2H_2O$ (**1**)

The starting materials $H_4SiMo_{12}O_{40}$ (1 mM, 183 mg), bpe (1 mM, 18 mg), $Cu(NO_3)_2 \cdot 3H_2O$ (2 mM, 48 mg), triethylamine (tea) (1 mM), and distilled water (9 mL) were mixed. The resulting suspension was stirred for 1 h and the pH was adjusted to 4.5 by 1 M NaOH and then sealed in an 18 mL Teflon-lined reactor. After heating six days at 160 °C, the reactor was slowly cooled to room temperature. Black–brown block crystals of **1** were filtered, washed with water, and dried at room temperature. Yield: *ca.* 34% based on Mo. Anal. Calcd for $C_{36}H_{36}N_6Cu_2SiMo_{12}O_{42}$ (2531) (%): C, 17.06; H, 1.18; N, 3.32; Cu, 5.05. Found (%): C, 17.03; H, 1.34; N, 3.29; Cu, 5.04.

2.3. Preparation of 1-CPE

Graphite powder (48 mg) and 8 mg of **1** were ground together by agate mortar and pestle to achieve a uniform mixture, and then 0.6 mL nujol was added with stirring. The homogenized mixture was packed into a glass tube with 1.2 mm inner diameter, and the tube surface was wiped with paper. Electrical contact was established with copper rod through the back of the electrode.

2.4. Photocatalysis

To investigate the photocatalytic activities of **1** as catalyst, the photodecomposition of Rhodamine-B (RhB) is evaluated under UV light irradiation through a typical process; the powder of **1** (50 mg) was mixed with 100 mL RhB solution [$1.0 \times 10^{-5} \text{ M L}^{-1} (C_0)$] in a beaker by ultrasonic dispersion for 10 min. The mixture was stirred for 0.5 h until the surface adsorption equilibrium was reached on the particles of **1**. Then, the mixture was stirred continuously under ultraviolet (UV) irradiation from a 125 W high pressure Hg lamp. Every 30 min, 3 mL of the sample was taken from the beaker, followed by several centrifugations to remove **1** and a clear solution was obtained for UV-vis analysis.

2.5. X-ray crystallographic study

Crystal data for **1** was collected on a Bruker SMART-CCD diffractometer with Mo-K α monochromated radiation ($\lambda = 0.71073 \text{ \AA}$) at 293 K. All structures were solved by direct methods and refined by full matrix least squares on F^2 using the SHELXTL crystallographic software package [30]. All non-hydrogen atoms were refined anisotropically. A summary of the crystallographic data and structural determination is provided in table 1. Selected bond lengths and angles for **1** are listed in table S1 (see online supplemental material at <http://dx.doi.org/10.1080/00958972.2015.1009907>).

3. Results and discussion

In crystal engineering, the control of self-assembly processes is still challenging to realize the target syntheses of the POMCPs. Many parameters such as initial reactants and their stoichiometry, pH, crystallization temperature, and pressure can affect the final structures. Subtle changes of each factor may cause alterations of the self-assembly process and

Table 1. Crystal data and structure refinements for **1**.^{a,b}

Empirical formula	$\text{C}_{36}\text{H}_{36}\text{N}_6\text{Cu}_2\text{SiMo}_{12}\text{O}_{42}$
Formula weight	2531
CCDC	1009372
Temperature (K)	293(2)
Wavelength (\AA)	0.71069
Crystal system	Monoclinic
Space group	<i>P</i> -1
<i>a</i> (\AA)	10.593(5)
<i>b</i> (\AA)	12.717(5)
<i>c</i> (\AA)	13.149(5)
α ($^\circ$)	71.106(5)
β ($^\circ$)	80.179(5)
γ ($^\circ$)	71.366(5)
<i>V</i> (\AA^3)	1583.6(11)
<i>Z</i>	1
D_{calcd} (mg m^{-3})	7.325
μ (mm^{-1})	3.068
<i>F</i> (0 0 0)	206.0
Goodness-of-fit on F^2	1.062
Final <i>R</i> indices [$I > 2\sigma(I)$]	$R_1 = 0.0620$, $wR_2 = 0.1269$
<i>R</i> indices (all data)	$R_1 = 0.0687$, $wR_2 = 0.1298$

$$^a R_1 = \frac{\sum ||F_o| - |F_c||}{\sum |F_o|}$$

$$^b wR_2 = \frac{\sum [w(F_o^2 - F_c^2)]}{\sum [w(F_o^2)]^{1/2}}$$

construct different structures. Thus, we have performed many parallel experiments *via* changing the pH and *trea*. When the pH is higher than 5, slurry precipitate can be obtained, and when the pH is lower than 4, only floccules can be observed. Additionally, *trea* is not necessary for construction of **1**.

Note that the oxidation state of copper was changed from the reactant Cu(II) to Cu(I) in the product, which was confirmed by valence sum calculations (BVS) [31]. Such a phenomenon is often observed in reaction of an N-containing ligand with Cu(II) under hydrothermal conditions. The BVS results show all molybdenums are in +6 oxidation state, consistent with the elemental analysis, coordination geometries and charge balance, confirming the structure analyses.

3.1. Structural description of the new POM-based compound

To explore the relationship between structures and properties, a detailed study was adopted in this POM-based hybrid compound. Single-crystal X-ray diffraction reveals that the asymmetric unit consists of one Cu⁺, one and a half bpe ligands, one [H₂SiMo₁₂O₄₀]²⁻ polyanion (abbreviated as {SiMo₁₂}), and one lattice water [figure 1(a)]. There is one crystallographically independent copper, which is three-coordinate in a “T-shape” geometry formed by two nitrogens from two bpe molecules and one oxygen from {SiMo₁₂} with bond distances of 1.908, 1.897, and 2.459 Å for Cu–N1, Cu–N2, and Cu–O2, respectively. The angles of N1–Cu–N2, O2–Cu–N1, and O2–Cu–N2 are 178.15°, 91.60°, and 89.56°, respectively. Two crystallographically independent bpe ligands are found in **1**, one links with two Cu centers and another is isolated. The {SiMo₁₂} cluster provides two terminal oxygens coordinating with Cu ions [figure 1(b)].

Supramolecular interactions play an important role in formation of hybrid materials. Cu ions covalently link with bpe molecules *via* Cu–N2 and Cu–N1 bonds forming wavy ([Cu (bpe)]_n) chains, and adjacent chains are connected forming the 1-D ladder-like chain *via* the {SiMo₁₂} clusters with covalent Cu–O2 bonds [figure 2(a)]. The chains fuse together forming the 3-D structure *via* Cu–O2#1 and Cu#1–O2 short interactions along the [1–10] axis and O8–O11 short interaction between SiMo₁₂ clusters along the *a* axis. The distances are 2.939 Å for Cu–O and 2.909 Å for O–O [figures 2(b) and 3]. The POM-based hybrid compound contains two-types of tunnels along the *a* axis and the [1–10] axis. More specifically, Cu centers link with {SiMo₁₂} clusters forming the 2-D POM-Cu inorganic layer (figure S1). Because the Cu centers and bpe molecules give rigid linear chains, the inorganic layers are

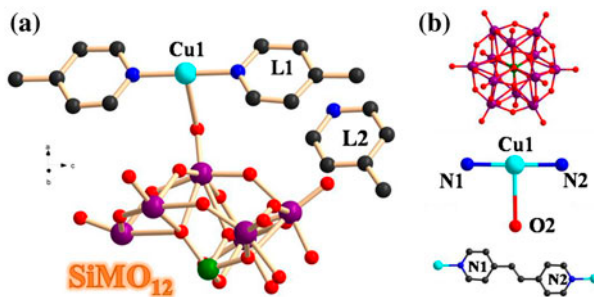


Figure 1. (a) Ball and stick representation of the unit cell of **1**. All hydrogens and water molecules have been omitted for clarity and (b) the coordination mode of SiMo₁₂ cluster, copper, and bpe molecule.

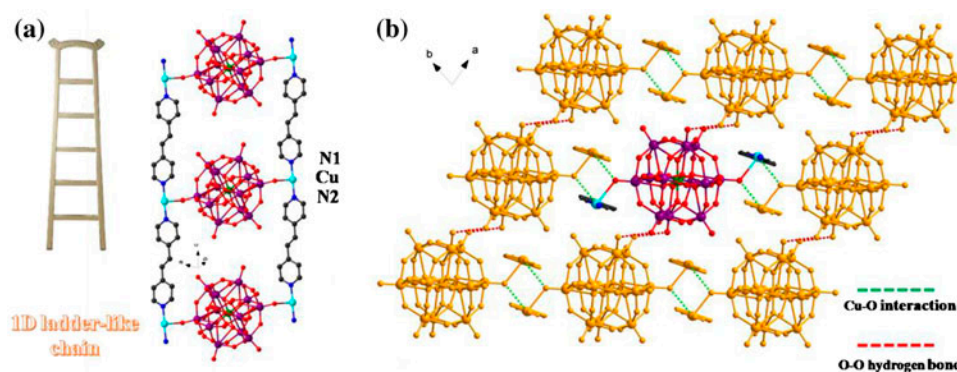


Figure 2. (a) Ball/stick representation of the ladder-like 1-D $[\text{Cu}(\text{bpe})]_n$ chain and (b) ball/stick representation of the 3-D structure of the hybrid compound along the c axis.

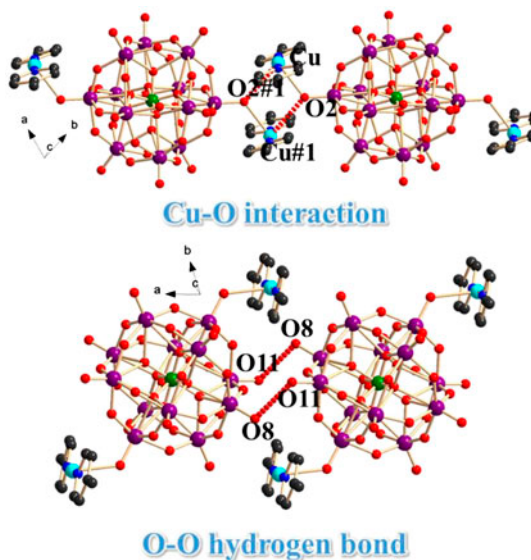


Figure 3. Ball/stick representation of the Cu–O₂ interaction between two ladder-like chains (upper) (symmetry code: #1: $1-x, 1-y, -z$) and O₈–O₁₁ interaction between two ladder-like chains (lower).

pillared by the linear $[\text{Cu}(\text{bpe})]_n$ chains, which give rise to the tunnels [figure 4(a)]. Isolated bpe molecules inhabit the tunnels and stabilize the structure (figure S2). From the topological view, if we assign the Cu (2-in-1) centers and SiMo_{12} clusters as four connected nodes, and the bpe molecules as connectors, the 3-D structure can be rationalized as a POMCPs network with CDS topology [32] and the Schläfli symbol is $(6^5 \cdot 8)$ [figure 4(c) and (d)].

3.2. FT-IR spectrum and thermal analysis

The IR spectrum of **1** is shown in figure S3. Characteristic bands at 961, 907, and 786 cm^{-1} are attributed to $\nu(\text{Mo}=\text{O})$, $\nu(\text{Si}-\text{O})$, and $\nu(\text{Mo}-\text{O}-\text{Mo})$ vibrations, respectively.

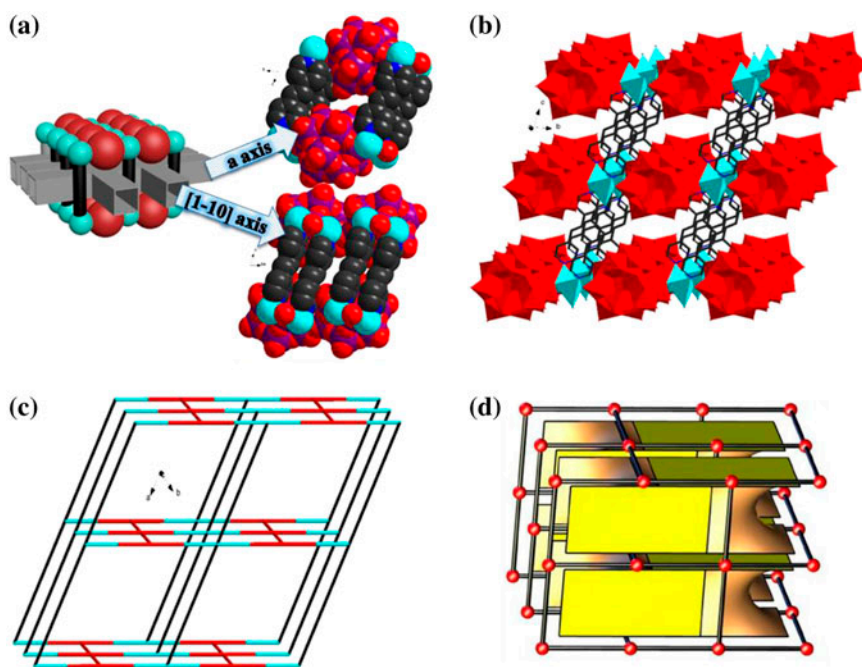


Figure 4. (a) Schematic diagram of the two types of tunnels; (b) combined polyhedral/ball/stick representation of the 3-D structure formed by inorganic layer and $[\text{Cu}(\text{bpe})_n]$ chains; view of the topology (c) and CDS net (d) of the compound. The blue nodes symbolize the Cu centers, the red nodes symbolize the $\{\text{SiMo}_{12}\}$ clusters and the black sticks symbolize the bpe molecules (see <http://dx.doi.org/10.1080/00958972.2015.1009907> for color version).

Bands at $1635\text{--}1104\text{ cm}^{-1}$ are attributed to bpe ligands. The thermal analysis of **1** (shown in figure S4) gives a total loss of 23.21% from 40 to 570 °C, which agrees with the calculated weight loss of 22.99%. The first weight loss of 1.67% at 40–250 °C corresponds to loss of one water per formula (Calcd 1.42%). The second weight loss of 21.54% at 250–570 °C arises from decomposition of organic ligands (Calcd 21.57%). These results further confirm the formula of **1**.

3.3. Electrochemical and electrocatalytic activities

The cyclic voltammetric (CV) behaviors of **1**-CPE were measured from +600 to –150 mV in 0.1 ML^{-1} H_2SO_4 aqueous solution at different scan rates. In the potential range, three pairs of redox peaks (I–I', II–II' and III–III') are observed [figure 5(a)] for **1**, ascribed to three consecutive redox processes of Mo ions, respectively, and the mean peak potentials $E_{1/2} = (E_{\text{pc}} + E_{\text{pa}})/2$ are +262, +141, and –52 mV. Note that there should exist a redox peak at 100–200 mV attributed to Cu(II)/Cu(I), which was not observed perhaps due to the overlap of Mo(VI)/Mo(V) redox peak. With increase in scan rate, the increasing extent of the anodic and cathodic peak currents is almost the same, and the peak potentials change gradually; the cathodic peak potentials shift toward the negative direction, the corresponding anodic peak potentials to the positive direction and the peak-to-peak separation between the corresponding cathodic and anodic peaks increases, but the average peak

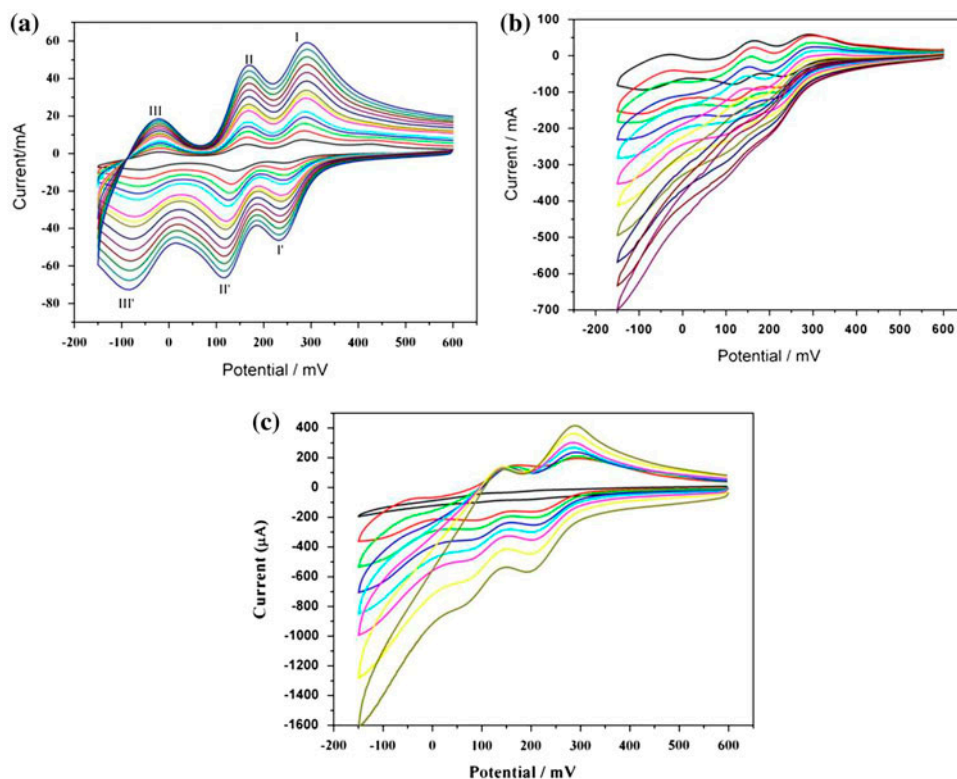


Figure 5. (a) The cyclic voltammograms of **1**-CPE in 1 M H₂SO₄ at different scan rates (from inner to outer: 30, 60, 90, 120, 150, 180, 210, 240, 270, 300, 330, 360, 390, 420 mV s⁻¹). Cyclic voltammograms of **1**-CPE in 1 M H₂SO₄ containing 1, 2, 3, 4, 5, 6, 7, 8, 9, 10 mM NaNO₂ (b) and 0, 2, 4, 6, 8, 10, 12 mM KBrO₃ (c). Scan rate: 100 mV s⁻¹.

potentials do not change. During the experiments, **1**-CPE showed higher stability than that of the conventional POM gel film electrode with the electrodes stable over 50 cycles at a scan rate 100 mV s⁻¹ and the current response remained almost unchanged. The remarkable stability for **1**-CPE should be ascribed to the insolubility of the hybrid POM nanoparticles.

POMs have been exploited in electrocatalytic reductions [33–35]. Herein, electrodes fabricated from POM nanoparticles and graphite were used to study electrocatalytic properties of **1** toward reduction in nitrite and bromate. The reduction of nitrite to ammonia involves a six-electron-eight-proton change. Owing to high overpotential required at most electrode surfaces for direct electroreduction of nitrite, no obvious response is observed for nitrite at bare CPE from +600 to -150 mV. Figure 5(b) shows the cyclic voltammogram of **1**-CPE at 100 mV s⁻¹ scan rate in acid solution containing nitrite. The result indicates that **1**-CPE has good electrocatalytic activity for reduction in nitrite. With addition of nitrite, all three reduction peak currents increase markedly while the corresponding oxidation peak currents decrease, suggesting that reduction in nitrite involves two-, four-, and six-electron-reduced species. The six-electron-reduced species has the largest catalytic activity towards reduction in nitrite. Figure 5(c) shows the cyclic voltammograms for electrocatalytic reduction of

bromate in acid solution. Unlike the electrocatalytic reduction of nitrite, the catalytic wave appears only for the third reduction waves, corresponding to four- to six-electron reduction, which indicates the catalytic activity for reduction in bromate mainly depends on the six-electron-reduced species.

3.4. Photocatalysis properties

The photodegradation of RhB assisted by **1** is shown in figure 6. For comparison, insoluble $(\text{NBu}_4)_4[\text{SiMo}_{12}\text{O}_{40}]$ was also employed in the same catalytic experiments. After irradiation for 300 min, the photocatalytic decomposition rates, defined as $1 - C/C_0$, are 91.3% for **1** and 67.2% for $(\text{NBu}_4)_4[\text{SiMo}_{12}\text{O}_{40}]$, respectively. When **1** was used, the absorption peak of the dye undergoes a large decrease, which indicates that formation of POM-based compound improves the photocatalytic performance of the POMs. The enhanced photocatalytic property may arise from the Cu-bpe subunits, which may act as photosensitizer under UV light, namely, promoting transition of electrons to POMs. Compound **1** possesses good degradation activity and may be a photocatalyst to decompose some organic dyes.

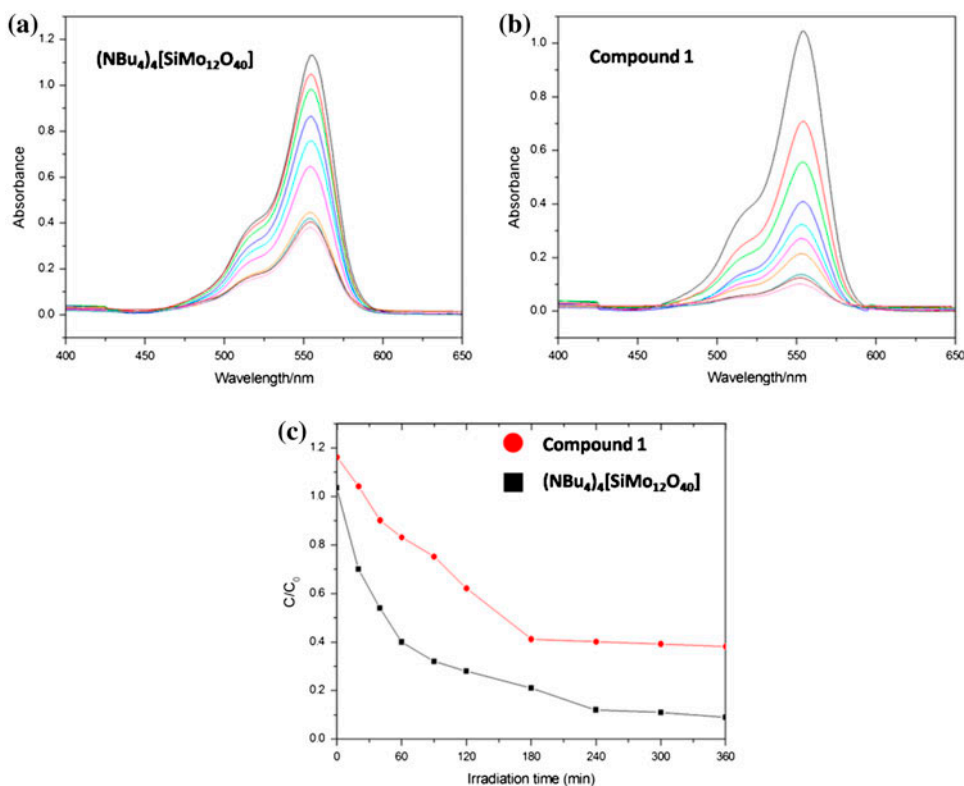


Figure 6. Evolution of UV-vis absorption spectra after 300 min of illumination for the photodegradation of RhB by $(\text{NBu}_4)_4[\text{SiMo}_{12}\text{O}_{40}]$ (a) and **1** (b); Kinetic of weight-based photocatalytic degradation of RhB dye by the catalysts (c).

4. Conclusion

By introducing the long rigid bpe into the POMs, a new POMCP with the stabilized lattice architecture has been reported. The 1-D ladder-like $\{[\text{Cu}(\text{bpe})]_2(\text{SiMo}_{12}\text{O}_{40})\}_n$ covalent chains link to each other *via* supramolecular interactions forming the whole structure, and the isolated bpe molecules stabilize the supramolecular compound. This material displays good electrocatalytic activity towards reduction in nitrite and bromate, and good photocatalytic activities for degradation of RhB dyes. The enhanced property may arise from the Cu-bpe subunits. This study will undoubtedly deepen our systematic understanding of the relationship between structures and properties of POMCPs. It is believed that more POMCPs with interesting structures and properties will be synthesized in the future.

Supplementary material

Crystallographic data and CCDC can be obtained free of charge from the Cambridge Crystallographic Data Center via www.ccdc.cam.ac.uk/data_request/cif. Tables of selected bond lengths (Å), bond angles (°) and figures, IR, TG for compound are provided in supporting information.

Funding

This work is financially supported by Graduate Innovation Foundation of Jiamusi University (LM2014_062).

References

- [1] O.M. Yaghi, M. O'Keeffe, N.W. Ockwig, H.K. Chae, M. Eddaoudi, J. Kim. *Nature*, **423**, 705 (2003).
- [2] M. Eddaoudi, J. Kim, N. Rosi, D. Vodak, J. Wachter, M. O'Keeffe, O.M. Yaghi. *Science*, **295**, 469 (2002).
- [3] S. Kitagawa, R. Kitaura, S. Noro. *Angew. Chem. Int. Ed.*, **43**, 2334 (2004).
- [4] B. Moulton, M.J. Zaworotko. *Chem. Rev.*, **101**, 1629 (2001).
- [5] L.J. Prins, J. Huskens, F.D. Jong, P. Timmerman. *Nature*, **398**, 498 (1999).
- [6] T. McGlone, C. Streb, D.L. Long, L. Cronin. *Adv. Mater.*, **22**, 4275 (2010).
- [7] T. McGlone, J. Thiel, C. Streb, D.L. Long, L. Cronin. *Chem. Commun.*, **48**, 359 (2012).
- [8] X.Y. Liu, H.L. Nie, L. Wang, R.D. Huang. *J. Coord. Chem.*, **66**, 444 (2013).
- [9] S.T. Zheng, J. Zhang, X.X. Li, W.H. Fang, G.Y. Yang. *J. Am. Chem. Soc.*, **132**, 15102 (2010).
- [10] J.Y. Niu, G. Wang, J.W. Zhao, Y.X. Sui, P.T. Ma, J.P. Wang. *Cryst. Growth Des.*, **11**, 1253 (2011).
- [11] X.L. Wang, H.L. Hu, G.C. Liu, H.Y. Lin, A.X. Tian. *Chem. Commun.*, **46**, 6485 (2010).
- [12] J.Q. Sha, L.J. Sun, E. Zheng, H.B. Qiu, M.Y. Liu, H. Zhao, H. Yuan. *J. Coord. Chem.*, **66**, 602 (2013).
- [13] J.Q. Sha, J. Peng, Y.Q. Lan, Z.M. Su, H.J. Pang, A.X. Tian, P.P. Zhang, M. Zhu. *Inorg. Chem.*, **47**, 5145 (2008).
- [14] Y.Q. Lan, S.L. Li, X.L. Wang, K.Z. Shao, D.Y. Du, H.Y. Zang, Z.M. Su. *Inorg. Chem.*, **47**, 8179 (2008).
- [15] A.X. Tian, J. Ying, J. Peng, J.Q. Sha, Z.M. Su, H.J. Pang, P.P. Zhang, Y. Chen, M. Zhu, Y. Shen. *Cryst. Growth Des.*, **10**, 1104 (2010).
- [16] J.Q. Sha, M.T. Li, J.W. Sun, P.F. Yan, G.M. Li, L. Zhang. *J. Asian Chem.*, **8**, 2254 (2013).
- [17] X.L. Wang, H. Zhang, E.B. Wang, C.W. Hu. *Mater. Lett.*, **58**, 1661 (2004).
- [18] X.L. Wang, Q. Zhang, Z.B. Han, E.B. Wang, Y.Q. Guo, C.W. Hu. *J. Electroanal. Chem.*, **563**, 221 (2004).
- [19] Z.G. Han, Y.L. Zhao, J. Peng, Y.H. Feng, J.N. Yin, Q. Liu. *Electroanalysis*, **17**, 1097 (2005).
- [20] K. Kalcher. *Electroanalysis*, **2**, 419 (1990).
- [21] X.L. Wang, E.B. Wang, Y. Lan, C.W. Hu. *Electroanalysis*, **14**, 1116 (2002).
- [22] D.E. Katsoulis. *Chem. Rev.*, **98**, 359 (1998).
- [23] T. Rüther, A.M. Bond, W.R. Jackson. *Green Chem.*, **5**, 364 (2003).
- [24] M.Q. Hu, Y.M. Xu. *Chemosphere*, **54**, 431 (2004).
- [25] E. Fontananova, L. Donato, E. Drioli, L.C. Lopez, P. Favia, R. d'Agostino. *Chem. Mater.*, **18**, 1561 (2006).
- [26] C.C. Chen, W. Zhao, P.X. Lei, J.C. Zhao, N. Serpone. *Chem.-Eur. J.*, **10**, 1956 (2004).

- [27] Y. Guo, Y. Wang, C. Hu, Y. Wang, E. Wang. *Chem. Mater.*, **12**, 3501 (2000).
- [28] G. Peng, Y. Wang, C. Hu. *Appl. Catal., A*, **218**, 91 (2001).
- [29] H. Salavati, N. Tavakkoli, M. Hosseinpoor. *Ultrason. Sonochem.*, **19**, 546 (2012).
- [30] (a) G.M.Sheldrick, *SHELX-97, Program for Crystal Structure Refinement*, University of Göttingen, Germany (1997); (b) G.M.Sheldrick, *SHELXL-97, Program for Crystal Structure Solution*, University of Göttingen, Germany (1997).
- [31] I.D. Brown, D. Altermatt. *Acta Crystallogr., Sect. B*, **41**, 244 (1985).
- [32] O.D. Friedrichs, M. O'Keeffe, O.M. Yaghi. *Solid State Sci.*, **5**, 73 (2003).
- [33] J.S. Dong, X. Xi, M. Tian. *J. Electroanal. Chem.*, **256**, 361 (1995).
- [34] B. Keita, A. Belhouari, L. Nadjo, R. Contant. *J. Electroanal. Chem.*, **381**, 243 (1995).
- [35] J.E. Toth, F.C. Anson. *J. Electroanal. Chem.*, **256**, 361 (1988).